

Article

# Open-Access Experiment Dataset for Fatigue Damage Accumulation and Life Prediction Models

Kris Hectors \* , Dennis Vanspeybroeck, Jelle Plets , Quinten Bouckaert  and Wim De Waele 

Laboratory Soete, Department of Electromechanical, Systems and Metal Engineering,  
Faculty of Engineering and Architecture, Ghent University, 9000 Ghent, Belgium

\* Correspondence: kris.hectors@ugent.be

**Abstract:** This work addresses the lack of focus on verification and comparison of existing fatigue damage accumulation and life prediction models on the basis of large and well-documented experiment datasets. Sixty-four constant amplitude, 54 two-level block loading, and 27 three-level block loading valid experiments were performed in order to generate an open-access, high-quality dataset that can be used as a benchmark for existing models. In the future, more experiments of various specimen geometries and loading conditions will be added. The obtained dataset was used for a study comparing five (non)linear fatigue damage and life prediction models. It is shown how the performance of several (non)linear damage models is strongly dependent on the considered material dataset and loading sequence. Therefore, it is important to verify models with a broad set of independent datasets, as many existing models show significant bias to certain datasets.

**Keywords:** fatigue; damage accumulation; experiments; metals; nonlinear damage; S-N curve; rotating bending; endurance



**Citation:** Hectors, K.; Vanspeybroeck, D.; Plets, J.; Bouckaert, Q.; De Waele, W. Open-Access Experiment Dataset for Fatigue Damage Accumulation and Life Prediction Models. *Metals* **2023**, *13*, 621. <https://doi.org/10.3390/met13030621>

Academic Editor: Tilmann Beck

Received: 23 February 2023

Revised: 13 March 2023

Accepted: 17 March 2023

Published: 20 March 2023



**Copyright:** © 2023 by the authors. Licensee MDPI, Basel, Switzerland. This article is an open access article distributed under the terms and conditions of the Creative Commons Attribution (CC BY) license (<https://creativecommons.org/licenses/by/4.0/>).

## 1. Introduction

Fatigue design principles were formulated nearly 150 years ago, since the time of Wöhler's early work on constant amplitude fatigue. These principles formed the foundation for the development of fatigue damage accumulation models that extended the S-N based fatigue design principle to components and structures subjected to variable amplitude cyclic loading. The linear damage rule (LDR), also called the Palmgren–Miner (PM) rule [1,2], is the most commonly used fatigue damage accumulation rule. Since the work of Miner in 1945 [2], the PM rule has been benchmarked to various fatigue experiments of specimens subjected to variable amplitude and block loading spectra. A comprehensive review of many of these testing programs and their results was carried out by Schütz [3]. The common conclusion of these experimental studies of lifetime estimations obtained with the Palmgren–Miner rule tend to be non-conservative for high–low block loading sequences ( $\sigma_{a,i} > \sigma_{a,i+1}$ ) and conservative for low–high ( $\sigma_{a,i} < \sigma_{a,i+1}$ ) block loading sequences [4]. For stochastic load spectra, lifetime estimations that are extremely non-conservative are not uncommon [3], up to a factor of 10 in some instances.

On a macroscopic level, load sequence and load interaction effects have been found to lead to nonlinear fatigue damage accumulation. The inherent linear nature of the Palmgren–Miner rule means that it cannot account for these effects. Consequently, the fatigue life estimations obtained using the Palmgren–Miner rule are generally unsatisfactory [5]. Considerable improvements have been made through the development of nonlinear damage accumulation models, but many require various parameters to be determined through extensive testing and have only been validated for very specific materials and loading conditions. Therefore, the Palmgren–Miner rule remains the standard for fatigue design. In 1998, Fatemi and Yang [6] presented a comprehensive review of fatigue damage accumulation and life prediction models. They highlighted the case-dependent performance of many models. Since their work, many more nonlinear damage accumulation models have

been published [7–9]. In 2021, authors of this paper published a review [10] that focused on fatigue damage accumulation and life prediction models published after the work of Fatemi and Yang. Most notably, new fatigue damage accumulation models are still published each year. A few of the most recent examples are the works of Pavlou [11], Bjørheim [12], Yu et al. [13], and Zhu et al. [14]. Nonetheless, an industry relevant breakthrough remains largely absent.

One of the primary conclusions of the review paper [10] was that most fatigue damage models have only been validated on relatively small experimental datasets. This makes it impossible to judge their generic performance. This issue was also raised by Patil et al. [15], who expressed their concern that many cumulative damage models have been and still are being developed using very small and very specific datasets. This was confirmed in the work of Hectors et al. [16]. These findings indicate that a focus shift from the development of new models to verification and comparison of existing models using large and well-documented experiment datasets is needed. Although this is in theory rather straightforward, a comprehensive comparison is hampered by the extremely limited number of well-documented datasets of block loading and random loading fatigue experiments available in the literature. The reasons are simple. Test specimens need to be machined to meet fine tolerances and subsequently polished to strict surface roughness requirements and, depending on the test conditions, experiments can last multiple days. Consequently, extensive test programs take months and are often prohibitively expensive.

There is now also the emerging domain of machine learning-based fatigue life prediction. Although this is currently mostly restricted to constant amplitude fatigue life prediction, some researchers have attempted to develop machine learning and deep learning models for variable amplitude fatigue life prediction. These developments are also further driving the need for extensive experiment datasets. In 2011, Gautham et al. [17] were the first to investigate data-driven methods to predict fatigue strength. Agrawal et al. [18] recognized the potential of this approach and decided to explore it further, which later led to development of an online machine learning tool by Agrawal and Choudhary [19] with the purpose of predicting the fatigue strength of steel. The fatigue strength prediction tool developed by Agrawal and Choudhary [19] was mentioned in the paper of Bock et al. [20], who reviewed the application of machine learning approaches for continuum mechanics. They concluded that the synergy between data and materials science holds significant potential. A similar conclusion was made by Sparks et al. [21] in their review paper on machine learning for structural materials.

However, the performance of machine learning models is limited to the training dataset size. Therefore, the most pressing need is additional data. As researchers venture into the development of data-driven variable amplitude fatigue life prediction models, the lack of qualitative datasets becomes even more clear. Gan et al. [22] proposed a kernel extreme learning machine (KELM) to estimate the remaining life of materials under two-step loading. Although their model demonstrated a superior performance compared to conventional damage accumulation theories, the database consisted of only 169 experimental results covering nine different materials collected from various sources. This again implicitly shows that the amount of suitable experimental data in the literature is limited. The work of Gan et al. [22] inspired Gao et al. [23] to further investigate remaining fatigue life prediction under two-step loading, comparing a number of machine learning models to conventional fatigue damage accumulation models. They found that all the machine learning models performed better than the conventional models. They used a dataset containing 328 experimental results for 12 different materials. Due to the sparsity of fatigue data and the cost and time requirements of fatigue tests, some researchers have started to focus their efforts on minimizing the necessary dataset size for machine learning training (e.g., [24,25]). Nonetheless, the primary factors influencing data-driven model performance are the size and number of features in the training dataset.

Based on a review of the current literature, it is clear that there is a general lack of experiment datasets, especially those that contain a detailed description of the individual

test results. This work aims to address this gap in the literature through the development of a well-documented dataset of block-loading experiments that can be used as a benchmark for (nonlinear) cumulative fatigue damage models. The goal of this work is not to develop a new cumulative damage or fatigue life prediction model, but to provide an open-access database that can be used for that purpose. In addition, five conventional cumulative damage models will be compared based on the newly obtained data. The results confirm the concerns that have already been raised in the past regarding the need for independent reassessment of cumulative damage and fatigue life prediction models and show the importance of introducing new datasets.

## 2. Materials and Methods

An extensive experimental program was devised for this work. All material used for the experimental program presented in this work was extracted from the web (at mid-thickness) of a decommissioned crane runway girder. The first step was a full characterization of the basic material properties. This was then followed by a full characterization of the constant amplitude fatigue properties (i.e., the S-N curve and endurance limit). Finally, a series of rotating bending fatigue experiments using two-level and three-level block loading spectra were performed.

The dimensions and surface roughness of every specimen were meticulously characterized and recorded. Knowledge of these features is expected to be essential for further advancement of the state of the art for both conventional (non)linear damage accumulation models and machine learning-based fatigue life estimation models as discussed in the introduction.

### 2.1. Basic Material Characterization

All specimens tested within the scope of this work are made of A37J steel, which is equivalent to today's S235 steel. The material characterization procedure and corresponding results have been reported in detail in [26] and are summarized here for the sake of completeness. Table 1 shows the chemical composition of the base metal. Tensile tests were performed in compliance with ASTM E8-21 [27] on an MTS 1000 kN servo-hydraulic testing rig. In total, six tensile specimens were extracted from two orthogonal directions, parallel to the rolling direction (RD) of the web plate the direction transverse to the rolling direction (TD), to characterize if the material exhibited any anisotropy. Detailed technical drawings of the specimens and their original location in the girder are available in the open-access dataset. Data of one tensile test were lost due to a data file corruption. Figure 1 shows the stress–strain curves obtained from the remaining five tensile tests. The raw data are available in the accompanying open-access dataset. The Young's modulus was measured for one tensile specimen of each material direction. The measurements were performed using two strain gauges, one at each side of the specimen, as recommended by the National Physics Laboratory [28]. Table 2 shows the results of the tensile tests. No significant differences in elastic–plastic properties were observed between the different specimens and material directions.

**Table 1.** Chemical composition of the steel. All values in wt. %.

C	Mn	Si	P	S	Cu	Ni
0.09	0.66	0.14	0.027	0.013	0.02	0.04
Cr	Mo	Ti	V	Al	Nb	
0.02	<0.01	0.005	<0.001	0.035	<0.001	

Finally, Vickers hardness maps were made using a Struers Duramin-40 Vickers hardness testing machine and a load of 9.81 N. The average across the two orientations was found to be  $117.74 \pm 8.39$  HV1. The Poisson's ratio of the base metal was not experimentally obtained and was assumed to be 0.28.

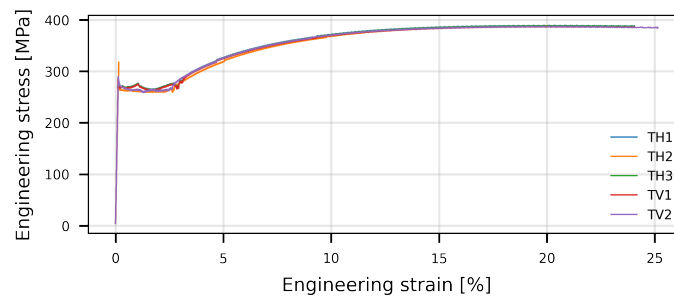


**Figure 1.** Stress–strain curves obtained from the tensile tests of the A37C steel specimens.

**Table 2.** Mean and standard deviation (across specimen orientation) of tensile properties of the base metal.

Tensile Property	Mean and Standard Deviation
Ultimate strength, $S_u$	$388.4 \pm 6.5$ MPa
Yield strength (0.2% offset, $R_{p0.2}$ )	$272.1 \pm 5.7$ MPa
Upper yield point	$294.5 \pm 11.7$ MPa
% Area reduction	$56.8 \pm 1.3\%$
Young's modulus, $E$	$207.4 \pm 1.8$ GPa

## 2.2. Fatigue Testing Setup and Specimen Configuration

In total of 160 specimens were extracted from the girder. Eighty specimens were extracted parallel to the rolling direction (RD) of the web plate and 80 from the direction transverse to the rolling direction (TD). The specimens were tested using an R.R. Moore rotating bending fatigue test setup. In the end, 145 valid experimental test results were obtained. For both material directions, the constant amplitude fatigue properties were first determined. The remaining specimens were tested with two-level and three-level block load sequences. Figure 2 shows a schematic of the test setup. All test specimens were produced in accordance with the ISO1143:2010 [29] standard for rotating bar bending fatigue. Figure 3 shows a technical drawing of the specimens that were produced.

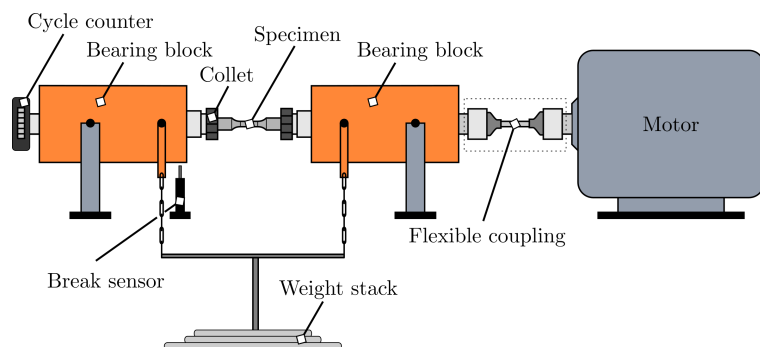


**Figure 2.** Schematic illustration of the R.R. Moore rotating bending fatigue setup.

It is well known that high cycle fatigue life is significantly influenced by the surface roughness. To minimize the effect of the surface roughness on the test results, the ISO1143:2010 [29] standard requires a mean surface roughness,  $R_a$ , less than  $0.2 \mu\text{m}$  with a final polishing direction along the test specimen axis. The specimens were manufactured on a CNC lathe, reaching an average as-machined roughness  $R_a$  of approximately  $0.8 \mu\text{m}$ . To obtain the required surface roughness, all specimens were manually polished with consecutively increasing grit sizes on a small-scale lathe. The first four polishing steps were performed using SiC-paper of 180, 240, 320, and 400 grit. Then a final polishing step with a P600 3M™ Trizact™ abrasive was performed. Before testing, each specimen was visually inspected for scratches. If no scratches were found, the roughness of the

specimen was measured at an arbitrary location using a Taylor Hobson Talysurf CCI 6000 white light interferometer to confirm if the surface roughness was satisfactory. Figure 4 shows one of the surface profile measurement results:  $R_a = 0.156 \mu\text{m}$  and  $S_{a,rough} = 0.176 \mu\text{m}$  were obtained.  $S_{a,rough}$  is the areal extrapolation of  $R_a$ . All roughness profile amplitude parameters were determined using a Gaussian filter with a cut-off wavelength of  $0.8 \text{ mm}$  in accordance with ISO3274:1996 [30].

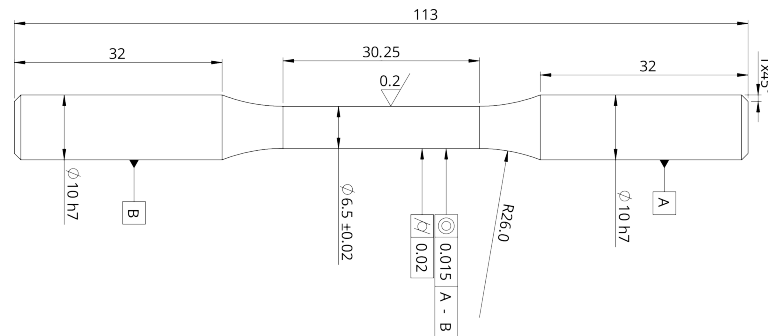


**Figure 3.** Illustration showing the specimen dimensions used in the experimental testing program, in accordance with ISO1143:2010 [29]. All dimensions are given in mm; the surface roughness is indicated in  $\mu\text{m}$ .

The final step was measuring the actual dimension of the specimen before testing and after polishing. The length was measured to an accuracy of  $0.01 \text{ mm}$ . The diameter was measured at three positions along the gauge length to an accuracy of  $1 \mu\text{m}$  with a Mitutoyo external micrometer. The smallest diameter value was then used to determine the required weight that had to be added to achieve the desired nominal stress amplitude.

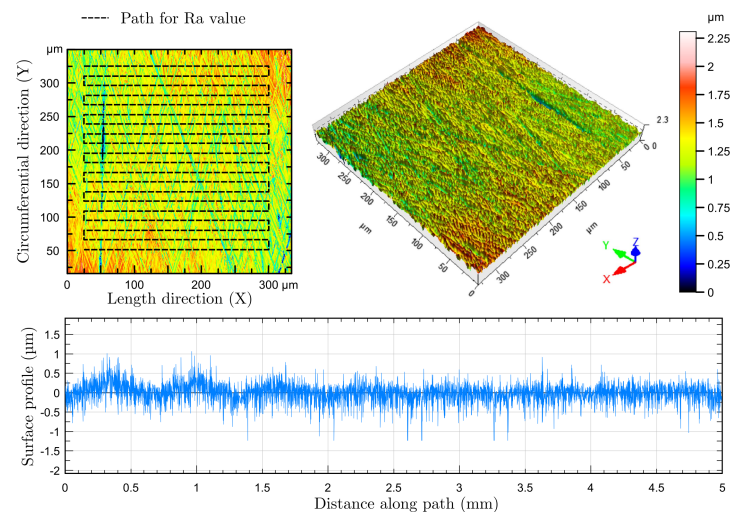


**Figure 4.** Surface profile measurement example of one of the tested fatigue specimens. Measurement performed with a white light interferometer.

### 2.3. Constant Amplitude Fatigue Properties

The data generation required for constructing an S-N curve was performed in accordance with ISO12107:2012 [31]. The consulted ISO standard discourages replicate data generation, recommending that the tests be allocated in double logarithmic stress level increments, as this allows one to define if the response is linear or curvilinear. The reason for this is that fatigue results tend to demonstrate more scatter at low stress levels, and double logarithmic spacing locates more specimens in the higher life regimes.

To define the lower bound limit that would result in failure within a reasonable time frame, the number of cycles corresponding to a run-out test was defined as  $10^7$ .

The endurance limit was determined using the staircase method as described by the ISO12107:2012 [31] standard. In this work, a stress amplitude step size of 2.5 MPa was used. Exploratory research requires a total of 15 valid tests to be performed such that a mean value and standard deviation of the endurance limit can be determined. The majority of the tests were performed at 66.7 Hz (4000 rpm). However for large stress amplitudes, initial trials showed that the specimen could reach temperatures high enough to influence the failure mechanism, thus requiring a reduced test frequency going as low as 500 rpm. On the contrary, a number of tests actually required a minimum of 33.3 Hz (2000 rpm), as lower test frequencies induced resonance effects that caused plastic deformation due to strong vibrations of the weight plate stack.

All valid results were post-processed in accordance with ISO12107:2012 [31]. A detailed example of the post-processing method can also be found in [16]. Figures 5 and 6 show the experimental data that were obtained from the constant amplitude rotating bending experiments. The individual test results are reported in Tables A1 and A2 and can also be download from the open-access database as detailed in the data availability statement at the end of this paper. Each data point corresponds to a single test where failure occurred before  $10^7$  cycles. For stress amplitudes above 260 MPa, a sudden considerable reduction in the fatigue strength was observed. Visual inspection of the fracture surfaces showed that the failure mechanism of these specimens was more closely related to low cycle fatigue than high cycle fatigue. Since the focus of this test program is high cycle fatigue, the remaining test specimens were allocated to stress levels below 260 MPa.

Staircase test series were performed separately for the two material directions. The staircase test results were post-processed as described in the aforementioned standard. A mean fatigue strength of  $233.75 \pm 1.13$  MPa was obtained for the vertical material direction and  $227.5 \pm 3.83$  MPa for the horizontal material direction.

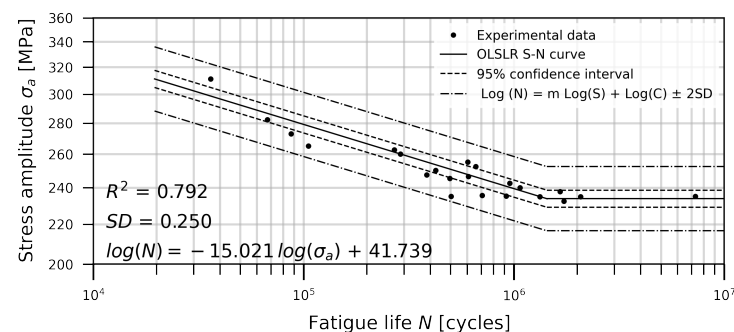


**Figure 5.** S-N curve obtained from the rotating bending experiments ( $R = -1$ ) for the specimens extracted from the transverse direction.

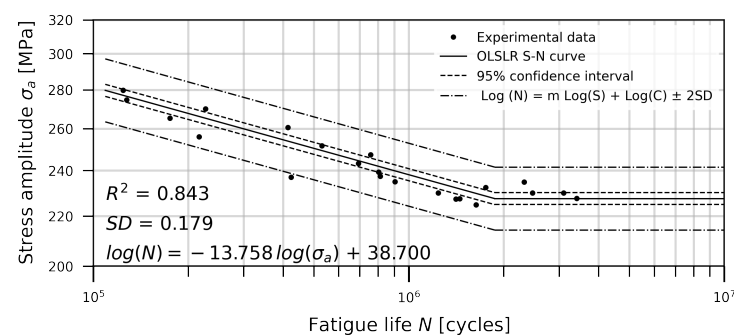


**Figure 6.** S-N curve obtained from the rotating bending experiments ( $R = -1$ ) for specimens extracted from the rolling direction.

The dash-dotted lines in Figures 5 and 6 represent the  $\pm 2$  standard deviation (SD) interval, with the lower bound (LB) generally used as a design curve. Standard deviations

of the least-squares fit are shown in the figures. Equations (1)–(6) are the equations for the best fit, lower, and upper bound confidence S-N curves for the transverse and rolling directions, respectively.

$$S_{a,TD} = 600.75 N^{-0.066573} \quad (1)$$

$$S_{a,TD,95\%LB} = 588.61 N^{-0.066573} \quad (2)$$

$$S_{a,TD,95\%UB} = 613.15 N^{-0.066573} \quad (3)$$

$$S_{a,RD} = 649.95 N^{-0.072684} \quad (4)$$

$$S_{a,RD,95\%LB} = 642.52 N^{-0.072684} \quad (5)$$

$$S_{a,RD,95\%UB} = 657.47 N^{-0.072684} \quad (6)$$

## 2.4. Block Loading Experiments

### 2.4.1. Test Program

In total, 81 specimens were tested under block loading. Of these, 54 specimens were subjected to two-level block loading series and 27 specimens to three-level block loading series. Twenty-nine of the two-level block loading tests were high-to-low (H–L) load tests and 25 were low-to-high (L–H) tests. Four of the H–L loaded specimens failed before the end of the first block. Technically, these can be considered to be constant amplitude experiments. In this work, these were, however, not considered in any of the following analyses, but they are reported in the appendices under two-level block loading for the sake of clarity. In addition, four specimens that were supposed to be subjected to three-level block loading failed in the second block. These were considered to be two-level block loading experiments in the model comparison study in Section 3 but are reported in Appendix C, which contains the results of the three-level block loading experiments.

Most fatigue datasets involving block loading that can be found in the open literature typically comprise experiments that were conducted with one or multiple blocks that had stress amplitudes corresponding to constant amplitude fatigue lives below  $10^4$  cycles. This corresponds to the low cycle fatigue regime. Since this work is solely focused on high cycle fatigue, stress amplitudes in the two- and three-level block loading test plans were defined to be consistent with those in the high cycle fatigue regime; i.e., stress amplitudes were chosen such that the corresponding constant amplitude fatigue life of each block's stress amplitude was larger than  $10^4$  cycles. All stress levels in the block loading tests were thus well below the yield point of the A37JC steel. More specifically, five test stress amplitudes, equally spaced between 260 MPa and 235 MPa, were chosen for this testing program.

For the two-level block loading experiments, the specimens were fatigued at a single stress amplitude (in rotating bending) to a desired percentage of total life as determined using Miner's rule and the S-N curves given in Equations (1) and (4). The specimens were then run to failure (fully fractured) or until the second load block exceeded  $10^7$  cycles at the final stress amplitude.

The three-level block loading experiments were performed similarly. The theoretically consumed fatigue life of the first two blocks, assuming linear damage accumulation, was the same. Finally, the test was run at a final stress amplitude until failure or the limit of  $10^7$  cycles.

### 2.4.2. Two-Level Block Loading: Results & Discussion

The results of the H–L experiments are reported in Tables A3 and A4, and the results of the L–H experiments are reported in Tables A5 and A6. The tables can be found in Appendix B. Overall, the experimental results are in line with the expectations based on previous experimental studies found in the literature regarding the tendency of Miner's rule to be conservative for L–H loading and non-conservative for H–L loading. This can be seen in Figure 7, which shows the remaining cycle ratio  $n_2/N_2$  as a function of the applied cycle ratio  $n_1/N_1$ . If points lay below the dashed line corresponding to Miner's rule, it means that life predictions based on Miner's rule are non-conservative and vice versa for

points laying above the dashed line. Not all tests followed the observed tendencies for L–H and H–L loading. Although some deviations are to be expected due to the scatter inherent in metal fatigue, it is remarkable that the (247, 235) load block tests showed completely opposite results. The (247, 235) sequence with  $n_1/N_1 = 0.25$  did not even result in failure. The latter could perhaps be classified as an outlier, but this does not explain the results of the other two (247, 235) sequence tests. At this stage, there is no conclusive evidence to identify why the tests of the (247, 235) sequence are not in line with general trends. This can most likely be attributed to the inherent scatter in fatigue life.

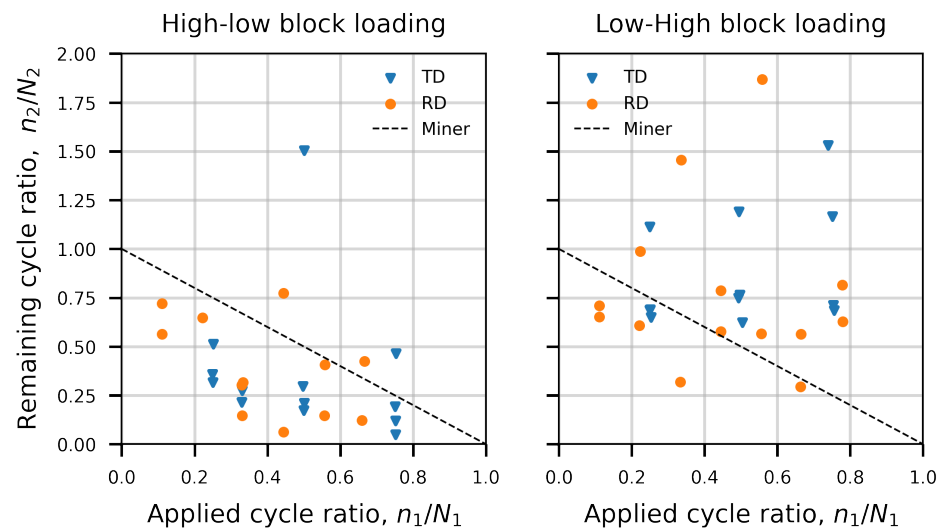


**Figure 7.** H–L (left) and L–H loading (right) experimental results. The dashed line corresponds to Palmgren–Miner’s rule. A distinction is made between specimens extracted from the transverse (TD) and rolling direction (RD).

The prediction of a model can only be as accurate as the data that are used for prediction. To account for the scatter that is inherent to fatigue, Figure 8 shows a comparison between Palmgren–Miner’s rule prediction and the experimental data, with error bars that correspond to the predictions based on the upper and lower bound 95% confidence interval S–N curves (Equations (2), (3), (5), and (6)). For the observations where the error bars intersect with the linear damage curve, the predictions can be considered adequate. Notably, the majority of the observations do not intersect with the linear damage curve. Surely this shows that Palmgren–Miner’s rule is not able to predict the damage accumulation behavior of the tested material.

Due to the shallow slope of the S–N curve that was obtained from the constant amplitude fatigue experiments, the range of stress amplitudes suitable for this study on high cycle fatigue was limited. As the difference between the largest possible stress amplitude ratio  $\sigma_{a1}/\sigma_{a2} = 260/235$  and the smallest ratio  $\sigma_{a1}/\sigma_{a2} = 242/235$  is rather limited, the study of the influence of load interaction effects was challenging. For a future study, it is advised to use a steel grade where high cycle fatigue is the governing damage mechanism for a wider range of stress levels.

#### 2.4.3. Three-Level Block Loading: Results and Discussion

The results of the three-level block loading experiments are reported in Tables A7 and A8 (see Appendix C). It can be seen that Palmgren–Miner’s rule is not consistently conservative or non-conservative. There are a number of very non-conservative results. On four occasions, the tests even resulted in failure before the end of the second load block. Each of these cases started with an H–L type sequence, where non-conservative estimations are to be expected. Nonetheless, these are very non-conservative (failure as early as  $\sum n_i/N_i = 0.48$ ). It can be seen that for both the High–Middle–Low (H–M–L) sequences in Table A8, the first two blocks were the same. The first two blocks both had a stress amplitude ratio

$\sigma_{a1}/\sigma_{a2} = 260/235$ . For the considered material, this corresponds to the largest possible stress amplitude ratio within the high cycle fatigue region. This strongly supports the idea that the stress amplitude ratio between subsequent loading blocks affects the severity of the non-linear effects.

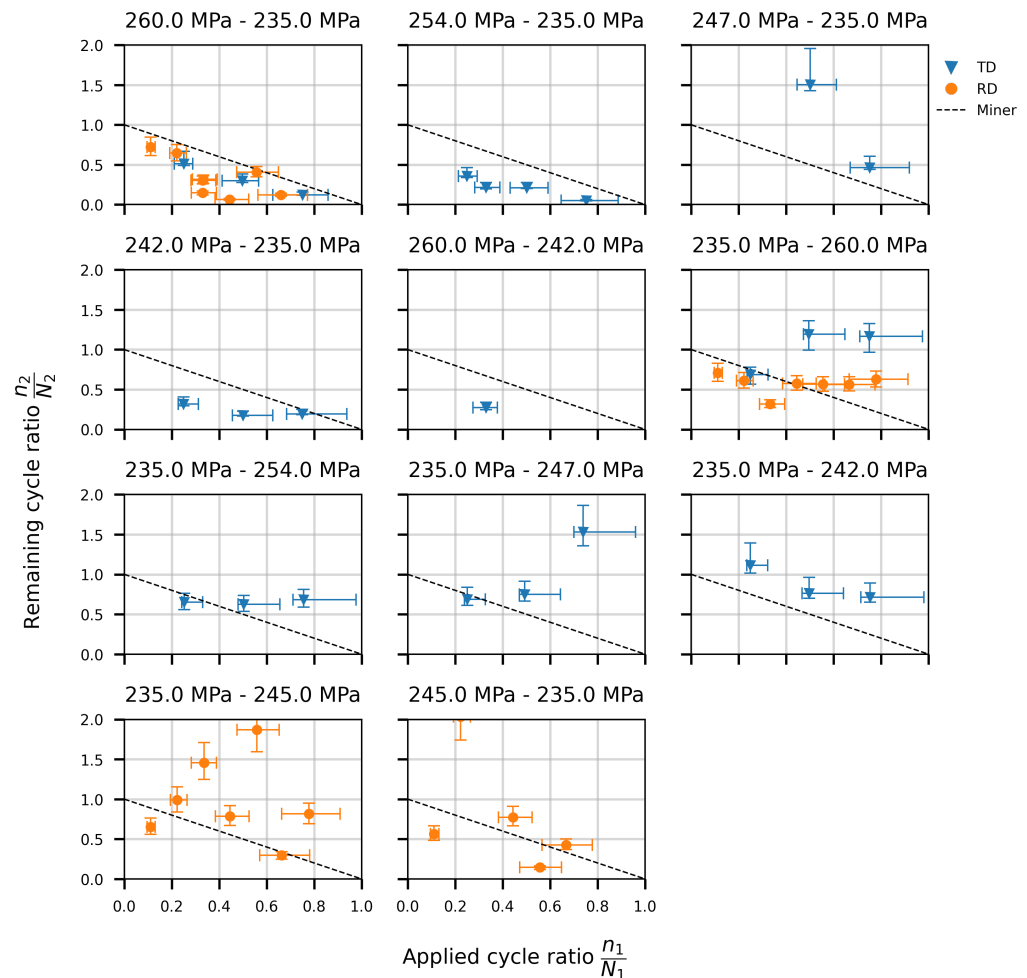


**Figure 8.** Comparison between the experimental two-level block loading data and Palmgren–Miner’s rule (dashed line), accounting for scatter on the fatigue life by considering the upper and lower bound 95% confidence interval S–N curves. A distinction is made between specimens extracted from the transverse (TD) and rolling direction (RD).

For the H–M–L sequence, intuitively  $\sum n_i/N_i < 1$  would be expected, analogue to a two-block H–L sequence. However, it is observed that this is not the case for all the experiments. More experiments of this type would be needed to make more profound conclusions. The results for the L–M–H tests are in line with the results from the two-block loading experiments. For the L–M–H experiments in Table A8, the experimental fatigue life of the third block is more than double the fatigue life as predicted by Miner for all three tests. The results suggest that Miner’s rule tends to be conservative for the L–M–H loading sequence.

Both the M–H–L and the M–L–H sequences show considerable scatter. Clear sequence effects cannot be identified. An extensive test program will be required to gauge how the stress amplitude ratio  $\sigma_{a,i}/\sigma_{a,i+1}$  between the subsequent blocks and the length of each block influence the fatigue damage accumulation rate.

### 3. Model Comparison

#### 3.1. Overview

In this section, the new experimental data are used to benchmark five (non)linear damage accumulation models and fatigue life prediction models. They were selected based on their prominence in the literature and simplicity regarding implementation. The latter remains one of the most important criteria for practicing engineers. A summary of the selected models can be found in [16]; for a detailed overview, the reader is referred to the original publications. The five selected models are Palmgren–Miner’s rule, the damage curve approach (DCA) by Manson and Halford [4], the modified damage curve approach (Mod. DCA) by Gao et al. [32], the fatigue driving stress (FDS) approach by Kwofie and Rahbar [33], and the damage stress model proposed by Mesmacque et al. [34]. All models are compared following the recommendations proposed in [16]. The analysis results are discussed separately for the two-level and three-level block loading experiments.

#### 3.2. Two-Level Block Loading Comparison

Table 3 shows the percentage of non-conservative ( $n_{2P}/N_2 > n_{2E}/N_2$ ) model estimations ( $P$ ) for the L–H and H–L loading datasets separately, considering all experiments ( $E$ ). All damage model predictions tend to the conservative side for L–H loading and to the non-conservative side for H–L loading. This is an important observation in a design context. Furthermore, the results in Table 3 also show that, for a considerable number of experiments, the results do not conform to these general observations. Thus, nonlinear damage models that inherently include this behavior can never achieve good predictions for all experimental results. Deviations from the almost universally agreed upon tendency of H–L to result in non-conservative Palmgren–Miner’s rule estimations and vice versa for L–H cannot be captured.

Comparing the results of the five considered damage accumulation models reported in Table 3, it can be observed that the Palmgren–Miner rule produces the most conservative predictions for L–H loading but the most non-conservative predictions for H–L loading. It is notable that none of the models performs considerably better than its counterparts. It should be noted that these results differ from those published in [16], where the same models were compared to experimental data already available in the literature. Hence, this confirms that the performance of these models can differ substantially for different experimental datasets.

**Table 3.** Percentage of non-conservative model estimations ( $n_{2P}/N_2 > n_{2E}/N_2$ ) for each model, for the two-level block loading experiments. *Exp* = experiments, *Est* = model estimation.

	Palmgren–Miner	DCA	Mod. DCA	FDS	DSM
L–H	30.77	42.31	42.31	34.62	34.62
H–L	80.77	69.23	73.08	76.92	76.92

To assess the model performance with respect to lifetime estimations that are consistently as close as possible to the real fatigue lifetime, a number of statistical measures are determined and compared. Seven conventional statistical metrics are considered. Four are relative to the experimental results, and three are absolute measures. The  $\text{Max}(n_{2P}/n_{2E})$ ,  $\text{Mean}(n_{2P}/n_{2E})$ ,  $\text{std}(n_{2P}/n_{2E})$ , and  $\text{RMSE}(n_{2P}/n_{2E})$  are the maximum value, mean value, standard deviation, and root mean square error of the estimated lifetime over the experimental lifetime, respectively. Ideally, the mean is close to one, the maximum is close to the mean, and the standard deviation and RMSE are close to zero. The  $\text{Mean}(n_{2P}/n_{2E})$  and  $\text{RMSE}(n_{2P}/n_{2E})$  are both measures of average model prediction error. For determination of the RMSE, the errors are squared before they are averaged; i.e., the RMSE more significantly penalizes larger errors. Since for fatigue lifetime estimation, larger errors can be considered disproportionately worse than small errors, the RMSE is the more important error measure in this case. It is, however, less intuitive than the  $\text{Mean}(n_{2P}/n_{2E})$ , which is

why the latter is also included. Apart from the relative measures, the mean and maximum absolute prediction errors and the absolute RMSE are reported to clearly quantify the prediction errors.

Table 4 summarizes the statistical analysis of the lifetime estimations for the two-block loading. The Palmgren–Miner rule performs worst for all calculated statistical metrics with the exception of the maximum absolute error. Conversely, the DCA and Mod. DCA are found to be the best performing models. In comparison to the results reported in [16], the discrepancies between the different models' performance are smaller in this work. However, the overall model performance ranking is the same as in [16].

**Table 4.** Statistical analysis of the selected damage accumulation model estimations for two-level block loading sequences presented in Section 2.4.2.

Model	PM	DCA	Mod. DCA	FDS	DSM
Max( $n_{2P}/n_{2E}$ )	8.91	5.97	6.22	8.03	7.42
Mean( $n_{2P}/n_{2E}$ )	1.50	1.29	1.31	1.44	1.39
std( $n_{2P}/n_{2E}$ )	1.49	0.99	1.03	1.34	1.22
RMSE( $n_{2P}/n_{2E}$ )	0.48	0.44	0.44	0.47	0.46
Mean absolute error [cycles]	315,998	256,369	260,029	294,885	287,407
Max. absolute error [cycles]	1,503,473	1,599,966	1,595,884	1,541,720	1,529,970
RMSE( $n_{2P}$ ) [cycles]	439,351	404,956	406,566	424,709	420,337

P = Prediction, E = Experimental, RMSE = Root Mean Square Error, std = Standard Deviation.

### 3.3. Three Level Block Loading

The statistical analysis of the three-level block loading experiments is summarized in Table 5. Compared to the two-level block loading, where the DSM model was one of the worst performing models, it actually performed best for the three-level block loading. This was also observed in [16]. Hence, for future studies that consider multi-level block loading spectra, the DSM should definitely be considered.

Notably, the FDS approach performs worse than Miner's rule. The part of the FDS damage function that accounts for interaction effects occurring when the stress level changes is based on the fatigue strength corresponding to the very first stress level that is applied to the specimen. Thus, even when the stress level changes from that of the second load block to that of the third load block, the interaction effect is based on the fatigue strengths corresponding to the first and third block stress levels. According to the authors of this paper, this makes no physical sense.

The Palmgren–Miner rule still exhibits considerably larger maximal and mean values and a standard deviation of ( $n_{3P}/n_{3E}$ ), compared to the DSM, DCA, and Mod. DCA. It does exhibit the lowest absolute errors, and the RMSE ( $n_{3P}/n_{3E}$ ) of Palmgren–Miner's rule is a shared best value. This shows that for block loading spectra with both high–low and low–high interactions, the non-linearity effects could even out. However, much larger datasets are required to make definitive conclusions on this.

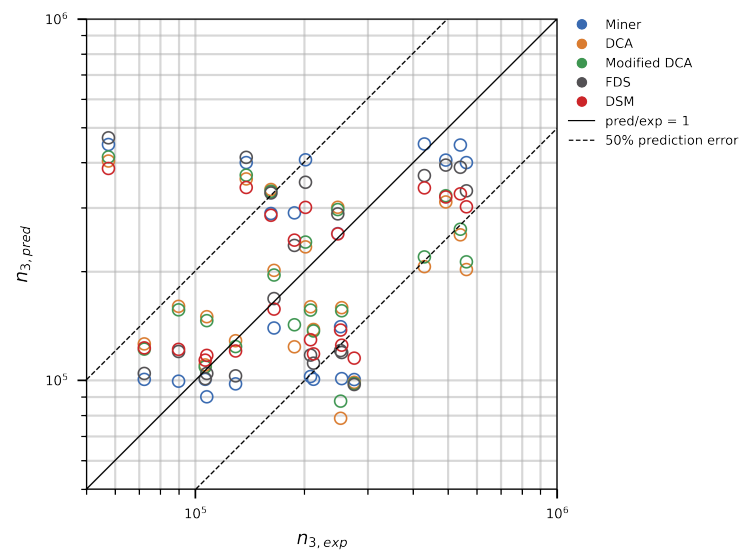
Overall, the DCA and Mod. DCA still perform better than the Palmgren–Miner rule. It should be noted that the Mod. DCA, which should obviously be an improvement on the original DCA, performs worse (albeit slightly) than the original DCA for both the two- and three-level block loading test series of the presented dataset.

Figure 9 shows the predicted versus experimental remaining fatigue life for the third loading block. It shows that there are considerable differences between the fatigue lifetime estimation of the studied models for individual cases. Overall, most of the model predictions are within 50% of the experimental results. It can also be seen in the figure that, for most experiments, the DSM is clearly the best performing model, which of course agrees with the descriptive statistics reported in Table 5.

**Table 5.** Statistical analysis of the selected damage accumulation model predictions based on the newly generated three-level block loading dataset.

Metric	Miner	DCA	Mod. DCA	FDS	DSM
$\text{Max}(n_{3P}/n_{3E})$	4.69	4.22	4.33	4.89	4.02
$\text{Mean}(n_{3P}/n_{3E})$	1.75	1.57	1.59	1.76	1.55
$\text{std}(n_{3P}/n_{3E})$	1.55	1.31	1.33	1.55	1.24
$\text{RMSE}(n_{3P}/n_{3E})$	0.29	0.31	0.30	0.29	0.29
Mean absolute error [cycles]	150,056	179,794	176,271	158,482	155,694
Max. absolute error [cycles]	1,082,126	1,219,470	1,204,285	1,108,759	1,187,200
$\text{RMSE}(n_{3P})$	265,102	303,412	299,319	274,531	282,386

P = Prediction, E = Experimental, RMSE = Root Mean Square Error, std = Standard Deviation.

**Figure 9.** Predicted versus experimental remaining fatigue life for the third loading block.

#### 4. Conclusions

This paper presented an experimental study of nonlinear fatigue damage accumulation followed by a comparative study of five fatigue damage accumulation and life prediction models. In this work, 145 valid rotating bending fatigue experiments were performed. Of these, 82 were block loading experiments, providing a considerable addition to the open-source state of the art. The main findings are summarized below.

- The two- and three-level block loading experiments showed that, even accounting for scatter on fatigue life by using the upper and lower bound 95% confidence intervals of the S-N curves, Miner's linear damage accumulation rule is not able to adequately describe the observed damage accumulation behavior, resulting in both conservative and non-conservative predictions.
- A comparative study of five prominent fatigue damage accumulation models showed that Miner's rule is consistently the worst performing model. It was found that for two-level block loading, the damage curve approach of Manson and Halford performed best. For three-level block loading, the DSM model of Mesmacque et al., which was one of the worst performing models for two-level block loading, performed best. This indicates that future experimental research should focus on multi-level block loading compared to two-level block loading. The latter, however, remains an important benchmark for gaining insight into the fundamental understanding of load sequence and load interaction effects.
- The main objective of this study was to create a comprehensive and reliable open-access database comprising high-quality data. Access to all the raw experimental data is available via the link provided in the data availability statement at the end of this paper.

The authors plan to continue augmenting this dataset with additional experimental findings in the future, thereby aiding the development of data-driven methods for fatigue life prediction. While the size of dataset currently presented is still insufficient, the authors intend to set a precedent for data collection and reporting standards.

**Author Contributions:** Conceptualization, K.H. and W.D.W.; methodology, K.H.; software, K.H.; validation, K.H. and W.D.W.; formal analysis, K.H.; investigation, K.H. and D.V.; resources, W.D.W.; data curation, K.H. and D.V.; writing—original draft preparation, K.H., D.V., J.P. and Q.B.; writing—review and editing, K.H., J.P., Q.B. and W.D.W.; visualization, K.H. and D.V.; supervision, K.H. and W.D.W.; project administration, W.D.W.; funding acquisition, W.D.W. All authors have read and agreed to the published version of the manuscript.

**Funding:** This research was funded by VLAIO project number 179P04718W.

**Data Availability Statement:** The database mentioned in this article is published in an open-access repository. It can be accessed with the following link: <https://doi.org/10.17605/OSF.IO/6Y5SD>. Please cite this paper when using the data of A37JC steel for your research.

**Acknowledgments:** The authors gratefully acknowledge the financial support from VLAIO (Flemish Agency for Innovation and Entrepreneurship), SIM (Strategic Initiative Materials) and IBN Offshore Energy through project ICON Safelife (179P04718W), and from the Energy Transition Fund of the Federal Public Service Economy through project MaxWind.

**Conflicts of Interest:** The authors declare no conflict of interest.

## Appendix A. Experimental Results Constant Amplitude Loading

**Table A1.** Experimental results constant amplitude loading, specimens extracted from the transverse direction.

Stress Amplitude [MPa]	Cycles to Failure	Test Frequency [RPM]
186.06	Run-out	4000
230.02	Run-out	4000
230.09	Run-out	4000
232.39	Run-out	4000
232.40	Run-out	4000
232.44	1,727,054	4000
232.48	Run-out	4000
232.48	Run-out	4000
232.64	Run-out	4000
232.76	Run-out	4000
234.83	2,077,810	4000
234.84	1,328,522	4000
234.98	1,072,703	4000
235.02	502,629	4000
235.13	7,292,489	4000
235.21	Run-out	4000
235.31	918,216	4000
235.61	705,992	4000
237.80	1,655,916	4000
240.08	1,068,136	4000
242.53	956,867	4000
245.35	495,745	3000
246.43	607,824	2000
247.38	384,489	4000
250.21	425,629	4000
252.35	659,037	1500
255.19	603,090	2000
260.15	288,380	2000
265.12	105,487	4000
273.02	87,287	3000
282.26	67,402	3000
311.15	36,145	500

Run-out: Stopped at  $10^7$  cycles without failure.

**Table A2.** Experimental results constant amplitude loading, specimens extracted from the rolling direction.

Stress Amplitude [MPa]	Cycles to Failure	Test Frequency [RPM]
222.67	Run-out	4000
224.86	1,634,316	4000
224.97	Run-out	4000
224.99	Run-out	4000
225.19	Run-out	4000
227.26	1,411,137	4000
227.26	Run-out	4000
227.46	Run-out	4000
227.53	Run-out	4000
227.55	3,407,330	4000
229.93	2,468,304	4000
229.95	Run-out	4000
229.95	Run-out	4000
230.00	1,241,237	4000
230.00	3,099,455	4000
232.43	1,755,321	4000
234.80	2,323,842	4000
234.98	904,263	4000
236.99	424,037	4000
237.36	812,867	4000
239.25	802,647	4000
243.26	693,499	4000
256.02	216,364	4000
260.59	414,138	1500
265.33	175,072	1500
269.98	226,824	1000
274.72	127,698	1000
279.69	124,317	500

Run-out: Stopped at  $10^7$  cycles without failure.

## Appendix B. Experimental Results Two-Level Block Loading

**Table A3.** Experimental results H-L block loading, specimens extracted from the transverse direction.

$\sigma_{a1}$ [MPa]	$\sigma_{a2}$ [MPa]	$n_{1E}$ [Cycles]	$n_{2E}$ [Cycles]	$\frac{n_1}{N_1}$	$\frac{n_{2E}}{N_2}$	$\sum \frac{n_{iE}}{N_i}$
260	235	73,001	678,288	0.25	0.51	0.76
260	235	145,370	396,487	0.50	0.30	0.80
260	235	218,053	160,192	0.75	0.12	0.87
254	235	103,219	477,423	0.25	0.36	0.61
254	235	136,246	282,973	0.33	0.21	0.55
254	235	206,433	280,271	0.50	0.21	0.71
254	235	309,651	66,195	0.75	0.05	0.80
247	235	157,057	Run-out	0.25	N/A	N/A
247	235	314,115	2,016,315	0.50	1.52	2.00
247	235	471,171	619,827	0.75	0.47	1.22
242	235	213,537	416,096	0.25	0.31	0.57
242	235	427,070	229,793	0.50	0.17	0.67
242	235	640,604	253,396	0.75	0.19	0.94

Run-out: Stopped at  $10^7$  cycles without failure, N/A: Not Applicable.

**Table A4.** Experimental results H–L block loading, specimens extracted from the rolling direction.

$\sigma_{a1}$ [MPa]	$\sigma_{a2}$ [MPa]	$n_{1E}$ [Cycles]	$n_{2E}$ [Cycles]	$\frac{n_1}{N_1}$	$\frac{n_{2E}}{N_2}$	$\sum \frac{n_{iE}}{N_i}$
245	235	75,045	675,049	0.11	0.56	0.67
260	235	33,135	864,860	0.11	0.72	0.83
245	235	150,092	2,433,365	0.22	2.03	2.26
260	235	66,266	772,804	0.22	0.65	0.87
245	235	225,134	Run-out	0.33	N/A	N/A
260	235	99,399	380,673	0.33	0.32	0.65
245	235	300,179	921,984	0.44	0.77	1.22
260	235	132,531	487,419	0.56	0.41	0.97
245	235	375,223	173,245	0.56	0.15	0.70
245	235	450,268	507,730	0.67	0.42	1.09
260	235	198,797	146,335	0.67	0.12	0.78
245	N/A	343,558 *	N/A	0.78	N/A	0.51
245	N/A	177,815 *	N/A	0.78	N/A	0.26
260	N/A	218,995 *	N/A	0.78	N/A	0.73
260	N/A	159,496 *	N/A	0.78	N/A	0.54

\*: Failed in first block. Run-out: Stopped at  $10^7$  cycles without failure, N/A: Not Applicable.

**Table A5.** Experimental results L–H block loading, specimens extracted from the transverse direction.

$\sigma_{a1}$ [MPa]	$\sigma_{a2}$ [MPa]	$n_{1E}$ [Cycles]	$n_{2E}$ [Cycles]	$\frac{n_1}{N_1}$	$\frac{n_{2E}}{N_2}$	$\sum \frac{n_{iE}}{N_i}$
235	260	331,857	199,470	0.25	0.69	0.94
235	260	663,712	344,260	0.50	1.18	1.69
235	260	995,571	340,910	0.75	1.17	1.92
235	254	331,857	268,888	0.25	0.65	0.90
235	254	663,713	258,245	0.50	0.63	1.13
235	254	995,569	282,793	0.75	0.68	1.44
235	247	331,856	432,468	0.25	0.69	0.94
235	247	663,712	469,699	0.50	0.75	1.24
235	247	995,570	963,602	0.75	1.53	2.27
235	242	331,858	944,726	0.25	1.11	1.36
235	242	663,713	654,593	0.50	0.77	1.26
235	242	995,571	605,047	0.75	0.71	1.47

**Table A6.** Experimental results L–H block loading, specimens extracted from the rolling direction.

$\sigma_{a1}$ [MPa]	$\sigma_{a2}$ [MPa]	$n_{1E}$ [Cycles]	$n_{2E}$ [Cycles]	$\frac{n_1}{N_1}$	$\frac{n_{2E}}{N_2}$	$\sum \frac{n_{iE}}{N_i}$
235	245	133,002	438,514	0.11	0.65	0.76
235	260	133,002	210,924	0.11	0.71	0.82
235	245	266,288	667,807	0.22	0.99	1.21
235	260	266,285	181,286	0.22	0.61	0.83
235	245	399,429	983,971	0.33	1.45	1.79
235	260	399,429	95,080	0.33	0.32	0.65
235	245	532,574	530,954	0.44	0.79	1.23
235	260	532,573	171,816	0.44	0.58	1.02
235	245	665,714	1,259,287	0.56	1.87	2.43
235	260	665,714	168,263	0.56	0.57	1.12
235	245	798,859	199,786	0.67	0.30	0.96
235	260	798,859	168,169	0.67	0.56	1.23
235	245	932,002	552,328	0.78	0.82	1.59
235	260	932,003	187,170	0.78	0.63	1.41

### Appendix C. Experimental Results Three-Level Block Loading

**Table A7.** Experimental results three-level block loading, specimens extracted from the transverse direction.

Type	$\sigma_{a1}$	$\sigma_{a2}$	$\sigma_{a3}$	$n_{1E}$	$n_{2E}$	$n_{3E}$	$\frac{n_1}{N_1}$	$\frac{n_{2E}}{N_2}$	$\frac{n_{3E}}{N_3}$	$\sum \frac{n_{iE}}{N_i}$
H-L-M	260	235	242	95,945	438,050	187,988	0.33	0.33	0.22	0.88
H-L-M	260	235	254	95,943	438,050	252,269	0.33	0.33	0.61	1.27
H-M-L	260	254	235	95,945	136,246	540,687	0.33	0.33	0.41	1.07
H-M-L	260	242	235	95,945	235,057 *	N/A	0.33	0.28	N/A	0.61
H-M-L	260	242	235	95,945	281,866	430,011	0.33	0.33	0.32	0.98
L-M-H	235	254	260	438,052	136,246	89,913	0.33	0.33	0.31	0.97
L-M-H	235	242	260	483,053	281,866	107,603	0.36	0.33	0.37	1.06
L-H-M	235	260	242	438,050	95,943	161,885	0.33	0.33	0.19	0.85
L-H-M	235	260	254	438,050	95,943	165,100	0.33	0.33	0.40	1.06
M-H-L	254	260	235	136,246	95,945	1,532,312	0.33	0.33	1.15	1.82
M-H-L	242	260	235	281,867	95,945	57,539	0.33	0.33	0.04	0.70
M-L-H	254	235	N/A	136,246	282,973 *	N/A	0.33	0.22	N/A	0.55
M-L-H	242	235	260	281,869	438,050	129,246	0.33	0.33	0.44	1.11

\*: Failed in second block. N/A: Not Applicable.

**Table A8.** Experimental results three-level block loading, specimens extracted from the rolling direction.

Type	$\sigma_{a1}$	$\sigma_{a2}$	$\sigma_{a3}$	$n_{1E}$	$n_{2E}$	$n_{3E}$	$\frac{n_1}{N_1}$	$\frac{n_{2E}}{N_2}$	$\frac{n_{3E}}{N_3}$	$\sum \frac{n_{iE}}{N_i}$
H-L-M	260	235	251	98,405	367,498 *	N/A	0.33	0.31	N/A	0.64
H-L-M	260	235	242	98,405	176,340 *	N/A	0.33	0.15	N/A	0.48
H-M-L	260	243	235	98,405	249,490	561,935	0.33	0.33	0.47	1.14
H-M-L	260	251	234	98,405	159,776	201,720	0.33	0.33	0.17	0.83
L-H-M	235	260	251	395,435	98,405	31 158	0.33	0.33	0.06	0.72
L-H-M	235	260	242	395,435	98,405	247 761	0.33	0.33	0.33	0.99
L-M-H	243	251	260	249,490	159,776	212,263	0.33	0.33	0.71	1.37
L-M-H	235	251	260	395,435	159,776	254,015	0.33	0.33	0.85	1.51
L-M-H	235	243	260	395,435	249,490	208,317	0.33	0.33	0.70	1.35
M-H-L	243	260	235	249,490	98,405	138,319	0.33	0.33	0.12	0.78
M-H-L	251	260	234	159,776	98,405	492,782	0.33	0.33	0.41	1.07
M-L-H	243	235	260	249,490	395,435	72,283	0.33	0.33	0.24	0.90
M-L-H	251	243	260	159,776	249,490	106,540	0.33	0.33	0.36	1.02
M-L-H	251	235	260	159,776	395,435	275,069	0.33	0.33	0.92	1.59

\*: Failed in second block. N/A: Not Applicable.

### References

1. Palmgren, A.G. Die Lebensdauer von Kugellagern (Life Length of Roller Bearings or Durability of Ball Bearings). *Z. Verines Dtsch. Ingenieure (ZVDI)* **1924**, *68*, 339–341.
2. Miner, M.A. Cumulative damage in Fatigue. *J. Appl. Mech.* **1945**, *12*, A159–A164. [[CrossRef](#)]
3. Schütz, W. A history of fatigue. *Eng. Fract. Mech.* **1996**, *54*, 263–300. [[CrossRef](#)]
4. Manson, S.S.; Halford, G.R. Practical implementation of the double linear damage rule and damage curve approach for treating cumulative fatigue damage. *Int. J. Fract.* **1981**, *17*, 169–192. [[CrossRef](#)]
5. Porter, T.R. Method of analysis and prediction for variable amplitude fatigue crack growth. *Eng. Fract. Mech.* **1972**, *4*, 717–736. [[CrossRef](#)]
6. Fatemi, A.; Yang, L. Cumulative fatigue damage and life prediction theories: A survey of the state of the art for homogeneous materials. *Int. J. Fatigue* **1998**, *20*, 9–34. [[CrossRef](#)]
7. Bandara, C.S.; Siriwardane, S.C.; Dissanayake, U.I.; Dissanayake, R. Fatigue failure predictions for steels in the very high cycle region—A review and recommendations. *Eng. Fail. Anal.* **2014**, *45*, 421–435. [[CrossRef](#)]
8. Santecchia, E.; Hamouda, A.M.S.; Musharavati, F.; Zalnezhad, E.; Cabibbo, M.; El Mehtedi, M.; Spigarelli, S. A Review on Fatigue Life Prediction Methods for Metals. *Adv. Mater. Sci. Eng.* **2016**, *2016*, 1–26. [[CrossRef](#)]

9. Jimenez-Martinez, M. Fatigue of offshore structures: A review of statistical fatigue damage assessment for stochastic loadings. *Int. J. Fatigue* **2020**, *132*. [[CrossRef](#)]
10. Hectors, K.; De Waele, W. Cumulative damage and life prediction models for high-cycle fatigue of metals: A review. *Metals* **2021**, *11*, 204. [[CrossRef](#)]
11. Pavlou, D. A deterministic algorithm for nonlinear, fatigue-based structural health monitoring. *Comput. Aided Civ. Infrastruct. Eng.* **2022**, *37*, 809–831. [[CrossRef](#)]
12. Bjørheim, F.; Pavlou, D.G.; Siriwardane, S.C. Nonlinear fatigue life prediction model based on the theory of the S-N fatigue damage envelope. *Fatigue Fract. Eng. Mater. Struct.* **2022**, *45*, 1480–1493. [[CrossRef](#)]
13. Yu, A.; Huang, H.Z.; Li, Y.F.; Yang, W.; Deng, Z. A modified nonlinear fatigue damage accumulation model for life prediction of rolling bearing under variable loading conditions. *Fatigue Fract. Eng. Mater. Struct.* **2022**, *45*, 852–864. [[CrossRef](#)]
14. Zhu, D.; Zhang, W.; Ding, Z. A modified fatigue damage model considering loading sequence effect. *Int. J. Damage Mech.* **2022**, *31*, 1027–1056. [[CrossRef](#)]
15. Patil, N.; Mahadevan, P.; Chatterjee, A. A constructive empirical theory for metal fatigue under block cyclic loading. *Proc. R. Soc. A Math. Phys. Eng. Sci.* **2008**, *464*, 1161–1179. [[CrossRef](#)]
16. Hectors, K.; Van Hecke, T.; De Waele, W. Method for statistical evaluation of cumulative damage models applied to block loading. *Fatigue Fract. Eng. Mater. Struct.* **2022**, *45*, 3319–3332. [[CrossRef](#)]
17. Gautham, B.P.; Kumar, R.; Bothra, S.; Mohapatra, G.; Kulkarni, N.; Padmanabhan, K.A. More efficient ICME through materials informatics and process modeling. In Proceedings of the 1st World Congress on Integrated Computational Materials Engineering, San-Francisco, CA, USA, 15 July 2011; John Library: Hoboken, NJ, USA, 2011; pp. 35–42. [[CrossRef](#)]
18. Agrawal, A.; Deshpande, P.D.; Cecen, A.; Basavarsu, G.P.; Choudhary, A.N.; Kalidindi, S.R. Exploration of data science techniques to predict fatigue strength of steel from composition and processing parameters. *Integr. Mater. Manuf. Innov.* **2014**, *3*, 90–108. [[CrossRef](#)]
19. Agrawal, A.; Choudhary, A. An online tool for predicting fatigue strength of steel alloys based on ensemble data mining. *Int. J. Fatigue* **2018**, *113*, 389–400. [[CrossRef](#)]
20. Bock, F.E.; Aydin, R.C.; Cyron, C.J.; Huber, N.; Kalidindi, S.R.; Klusemann, B. A review of the application of machine learning and data mining approaches in continuum materials mechanics. *Front. Mater.* **2019**, *6*, 110. [[CrossRef](#)]
21. Sparks, T.D.; Kauwe, S.K.; Parry, M.E.; Tehrani, A.M.; Brgoch, J. A review of machine learning for structural materials. *Annu. Rev. Mater. Res.* **2020**, *50*, 27–48. [[CrossRef](#)]
22. Gan, L.; Zhao, X.; Wu, H.; Zhong, Z. Estimation of remaining fatigue life under two-step loading based on kernel-extreme learning machine. *Int. J. Fatigue* **2021**, *148*, 106190. [[CrossRef](#)]
23. Gao, J.; Wang, C.; Xu, Z.; Wang, J.; Yan, S.; Wang, Z. Gaussian process regression based remaining fatigue life prediction for metallic materials under two-step loading. *Int. J. Fatigue* **2022**, *158*, 106730. [[CrossRef](#)]
24. Karniadakis, G.E.; Kevrekidis, I.G.; Lu, L.; Perdikaris, P.; Wang, S.; Yang, L. Physics-informed machine learning. *Nat. Rev. Phys.* **2021**, *3*, 422–440. [[CrossRef](#)]
25. Gan, L.; Wu, H.; Zhong, Z. On the use of data-driven machine learning for remaining life estimation of metallic materials based on Ye-Wang damage theory. *Int. J. Fatigue* **2022**, *156*, 106666. [[CrossRef](#)]
26. Hectors, K.; Chaudhuri, S.; Waele, W.D. Fracture mechanics and hot spot stress-based fatigue life calculation: Case study for a crane runway girder. *Fatigue Fract. Eng. Mater. Struct.* **2022**, *45*, 2662–2675. [[CrossRef](#)]
27. ASTM E8/E8M-21; Standard Test Methods for Tension Testing of Metallic Materials. ASTM International: West Conshohocken, PA, USA, 2021. [[CrossRef](#)]
28. Lord, J.D.; Morrell, R. *Elastic Modulus Measurement*; Measurement Good Practice Guide No. 98; National Physical Laboratory: Teddington, England, 2016.
29. Technical Committee ISE/101/6. *BS ISO 1143:2010 Metallic Materials—Rotating Bar Bending Fatigue Testing*, 2nd ed.; British Standards Institution: London, UK, 2010.
30. Technical Committee ISO/TC 213. *ISO 3274:1996/COR 1:1998: Geometrical Product Specifications (GPS)—Surface Texture: Profile Method—Nominal Characteristics of Contact (Stylus) Instruments*; British Standards Institution: London, UK, 1998.
31. Technical Committee ISO/TC 164/SC 4. *ISO 12107: Metallic Materials—Fatigue Testing—Statistical Planning and Analysis of Data*, 2nd ed.; International Organization for Standardization: Geneva, Switzerland, 2012.
32. Gao, H.; Huang, H.Z.; Zhu, S.P.; Li, Y.F.; Yuan, R. A modified nonlinear damage accumulation model for fatigue life prediction considering load interaction effects. *Sci. World J.* **2014**, *2014*, 164378. [[CrossRef](#)]
33. Kwofie, S.; Rahbar, N. A fatigue driving stress approach to damage and life prediction under variable amplitude loading. *Int. J. Damage Mech.* **2013**, *22*, 393–404. [[CrossRef](#)]
34. Mesmacque, G.; Garcia, S.; Amrouche, A.; Rubio-Gonzalez, C. Sequential law in multiaxial fatigue, a new damage indicator. *Int. J. Fatigue* **2005**, *27*, 461–467. [[CrossRef](#)]

**Disclaimer/Publisher’s Note:** The statements, opinions and data contained in all publications are solely those of the individual author(s) and contributor(s) and not of MDPI and/or the editor(s). MDPI and/or the editor(s) disclaim responsibility for any injury to people or property resulting from any ideas, methods, instructions or products referred to in the content.